Controlled Production of Elastin-like Recombinamer Polymer-based Membrane at a Liquid-liquid Interface by Click Chemistry

Miguel González-Pérez,[1] Israel González de Torre,[1] Matilde Alonso,[1] José Carlos Rodríguez-Cabello[1]*

[1]BIOFORGE (Group for Advanced Materials and Nanobiotechnology), CIBER-BBN, University of Valladolid, 47011 Valladolid, Spain

KEYWORDS: elastin-like recombinamers, membranes, click chemistry, liquid-liquid interface

*Corresponding author. roca@bioforge.uva.es

ABSTRACT

Diffusion of organic and inorganic molecules controls most industrial and biological processes occurring at liquid phase. Even though many efforts have been devoted for the design and operation of large scale purification systems, diffusion devices with adjustable biochemical characters have remained aside. In this regard, micrometer bioinspired membranes with tunable diffusion properties have been engineered by covalent crosslinking of two elastin-like recombinamers (ELRs) at a liquid-liquid interface. The selected covalent approach provided the fabricated ELR-membranes with structural support while, modulating the concentration of the

employed polypeptides, conferred a direct control over the thickness, pore size and diffusive properties for a large window of molecular weights (4-150 kDa). The recombinant and versatile nature of the employed proteinaceous building blocks further opens chances for engineering bioactive motifs within the membrane scaffold widening their applicability in the biological field.

1. INTRODUCTION

Regulating the diffusion of molecules serves functions of paramount importance, from the purification of aqueous[1] and organic phases[2], to determining the biological activity of cells, tissues and organs in living species[3]. Although filtration and exclusion systems have been widely developed for industrial applications[4], further efforts need to be undertaken for designing biotunable diffusion devices that effectively integrate and comply with the intricate biological demands. The unique environment found in living organisms, in terms of mechanical properties[5] and wide range of biologically relevant molecules, i.e. small nutrients to large signaling factors and antibodies, restricts the array of materials to be employed for the fabrication of functional devices. In this sense, bioinspired hydrogels may serve as suitable scaffolds for developing membrane-like barriers that mimic the diffusive properties of native extracellular matrixes[6].

Intended for developing a versatile technology for fabricating resilient and highly biotunable diffusion membranes, elastin-like recombinamers (ELRs) have been investigated. These genetically engineered polypeptides, resembling the hydrophobic and intrinsically disordered region of the extracellular protein elastin[7], are designed to recapitulate the reversible thermoresponsive self-assembly in aqueous media[8]. Above a given temperature, known as transition temperature or "T_t"[9], ELR chains coacervate hydrophobically acquiring the characteristic flexibility and elastic recoil of the elastin[10, 11]. Furthermore, the recombinant origin

of this family of proteins, combined with their highly tailorable nature, offers encoding the required bioactive domains for addressing the aimed application[12].

In order to control the membrane thickness, pore size distribution, and so, diffusion properties, a two-phase system was selected for the fabrication of the ELR-based entity. As described, liquid interfaces have shown the ability to physically self-assemble ELRs into thin structures once in combination with polysaccharides[13], amphiphilic peptides[14, 15] and, recently, graphene oxide[16]. However, no technology has been explored for manufacturing, at a liquid-liquid interface, adjustable in thickness, porosity and diffusion micrometer and easy to manipulate membranes from ELRs alone.

A feasible approach, for reinforcing the mechanical properties of the intended thin ELR-membranes, consists in employing covalent crosslinkable domains. Among the available library, the catalyst-free [3 + 2] dipolar cycloaddition was selected as the most suitable approach for engineering the ELR matrix[17, 18]. This technology, apart from exhibiting an elevated orthogonality and short reaction time, has demonstrated a high biocompatibility with cells and complex culture media[19, 20], avoiding unexpected complications when facing biological studies.

In this sense, we biosynthesized and chemically modified two ELRs in order to include complementary click reacting groups for fabricating the diffusion-tailorable membrane. The structural VKV, intended to be contained in an organic water-immiscible phase, and the SKS, bearing RGD cell-adhesive domains and showing an elevated T_t for remaining dissolved in an aqueous phase upon fabricating the ELR-membrane at room temperature (r.t.). Once put in contact, a spontaneous crosslinking reaction occurred at the liquid-liquid interface leading the formation of a thin ELR-membrane. Recording the concurring events at the two-phase interface allowed

studying the growth of the structures with time while, by physical characterization, a direct relationship between the employed concentrations and the thickness, porosity, mechanical and diffusion properties was reported.

In summary, the designed strategy describes the fabrication of thickness, pore size and diffusion tailored ELR-membranes. Their intrinsic translucency along with the exhibited mechanical properties and high versatility of the employed elastin-like recombinamers evidences a promising technology for developing diffusion devices adjusted to need.

2. MATERIALS AND METHODS

2.1 Materials

2-azidoethyl (2,5-dioxopyrrolidin-1-yl) carbonate and (1R,8S,9S)-bicyclo[6.1.0]non-4-yn-9-ylmethyl succinimidyl carbonate were obtained from GalChimia (A Coruña, Spain). 96 Well Half-Area Microplate were acquired from Corning (NY, USA). 3 mL glass vials with 10 mm inner diameter, circular cover glasses of 15mm diameter, 1,5 mL Pierce microcentrifuge tubes and plastic Petri dish Nunc 35 mm diameter were purchased from Thermo Scientific (Toronto, ON, Canada). Tailored Franz cells were acquired from Afora (Barcelona, Spain). Deuterated dimethyl sulfoxide (DMSO-*d6*), dimethyl sulfoxide (DMSO), acetone, diethyl ether, ethanol (EtOH), n-butanol (BuOH), dichloromethane, ethyl acetate, xylene, cyclohexanone, 1-pentanol, 3-pentanone, ethyl acetoacetate, chloroform and 4 kDa, 20 kDa, 40 kDa, 70 kDa, and 150 kDa FITC-dextran were obtained from Sigma-Aldrich (San Luis, MO, USA).

2.2 ELRs bioproduction and characterization

Two ELRs were produced herein, a structural recombinamer called VKV previously described by I. González de Torre et al.[21] and an ELR bearing both RGD cell-adhesive motifs and serine groups referred to as SKS. The complete sequence of these polypeptides with a molecular weight of 60.5 and 82.5 kDa is detailed below:

MESLLP VG VPGVG $[VPGKG\ (VPGVG)_5]_{23}$ VPGKG $(VPGVG)_3$ VPGV

MESLLP $[(VPGVG\ VPGSG\ VPGVG\ VPGKG\ VPGVG\ VPGSG\ VPGVG)_2$ VAVTGRGDSPASSGGGGSGGGGSGGGGS $(VPGVG\ VPGSG\ VPGVG\ VPGKG\ VPGVG\ VPGSG\ VPGVG)_2]_6$ V

The production of these two ELRs was performed using standard genetic-engineering techniques[22]. Their purification consisted of several cycles of temperature and salt-dependent reversible precipitations by centrifugation, below and above their transition temperature (T_t), making use of the intrinsic thermal behavior of these compounds[23]. The obtained ELRs were dialyzed against ultrapure water (Millipore, Burlington, MA, USA) and freeze-dried. The purity and molecular weight of the ELRs were verified by comparison against an unstained protein molecular weight marker (Fermentas, Waltham, MA, USA) by sodium dodecyl sulphate polyacrylamide gel electrophoresis (SDS-PAGE) and by matrix assisted laser desorption/ionization time-of-flight (MALDI-TOF) mass spectrometry using a Bruker Daltonics Autoflex Speed Instrument (Bruker, Billerica, MA, USA). Amino acid composition analysis was performed by high performance liquid chromatography 1200 Series (Agilent Technologies, Santa Clara, CA, USA). Finally, additional characterization of ELRs was accomplished using Fourier-transform infrared spectroscopy employing a Bruker Tensor 27 (Billerica, MA, USA), differential scanning calorimetry by a Mettler Toledo DSC822e (Columbus, OH, USA) and proton nuclear

magnetic resonance by a Varian AV-400 (Agilent Technologies, Santa Clara, CA, USA) (Figure S1).

2.3 ELRs modification and characterization

A click catalyst-free reaction was the preferred covalent crosslinker for intertwining the ELR chains into membranes. As such, azide and cyclooctyne groups were used for labelling the SKS and VKV ELRs, respectively. The synthesis of azide-modified SKS ELR was done by transformation of the ε-amine group in the lateral lysine chain as follows: A solution of 2-azidoethyl (2,5-dioxopyrrolidin-1-yl) carbonate in DMSO was added to a solution of the SKS ELR in DMSO and the resulting mixture was stirred at r.t. for 48 h. After this time, diethyl ether was added to the mixture to give a white precipitate, which was dried under reduced pressure and dissolved in ultrapure water. The aqueous solution was dialyzed against ultrapure water and freeze-dried to yield a white recombinamer (SKS-azide). An 75% modification of the SKS lysine residues was confirmed by characterizing the azide modified version by MALDI-TOF, FTIR, DSC and ^{1}H NMR techniques (Figure S2).With regard to the VKV-cyclooctyne version a procedure found in the literature was followed[21].

2.4 Solubility/miscibility studies

2 mg of VKV-cyclooctyne ELR modified version contained in a 1,5 mL Pierce microcentrifuge tube were assayed against a set of single and mixed organic solvents observing the homogeneity of the final solution after vortexing. A visual evaluation of the presence or absence of precipitated recombinamer at the bottom of the tube allowed determining the dissolving capacity of the selected solvents. These tests were followed by the addition of ultrapure water. Again, after vortexing the mixture, a visual examination enabled to estimate the appearance of a two-phase system with time

or, on the contrary, a homogeneous solution. The mixture that dissolved the VKV-cyclooctyne and was immiscible with water was selected to be employed in the following experiments where both ELRs, SKS-azide contained in the aqueous solution and VKV-cyclooctyne in the organic phase, were put in contact in a custom-made cylindrical device.

2.5 Membrane formation and microscopic characterization

A customized cylinder (Ø = 16 mm) for mixing the organic and the aqueous phase creating a circular interface was designed. This device was equipped with a plunger seal and a hole specifically located on the side for facilitating the isolation of the formed membrane and the removal of the lower phase, respectively.

Two different polymeric solutions were prepared by dissolving at the same concentration the modified ELRs, SKS-azide and VKV-cyclooctyne, in ultrapure water and 23% DMSO in BuOH, respectively. Prior to the addition of both solutions, a circular cover glass was introduced in the container while the side hole remained covered during the formation process. Following, an equal volume of each solution was sequentially added in the designed cylindrical device. In order, the denser phase containing the SKS-azide (aqueous) was poured into the adapted system followed by the gently addition of the correspondent organic phase containing the VKV-cyclooctyne (23% DMSO in BuOH) providing a plain mix and disrupting as little as possible the water phase surface. Consecutively, polypeptide chains were allowed to react for 30 minutes at r.t. resulting in the formation of an ELR-membrane at the interface.

Once completed the reaction, the upper organic phase was smoothly retrieved, the ELR-membrane was carefully detached from the device wall and the aqueous phase was removed through the hole found beneath the menisci. The ELR-membrane was extracted from the top through the application

of a gentle force to the plunger. During this stage, the previously introduced circular cover glass emerged extending and dragging the outstretched membrane over it. ELR-membranes were prepared at four different concentrations, namely 50, 25, 10 and 5 mg mL^{-1}, for the study.

2.5.1 Real time formation

A system consisting of a cylindrical glass vial (Ø = 10 mm) and a magnifying glass (Leica DMS1000 B TL5000, Wetzlar, Germany) focused at the liquid-liquid interface, was employed for visualizing the ELR-membrane formation with time (see representative videos in supporting information).

2.5.2 Environmental scanning electron microscopy (ESEM)

ELR-membranes were mounted on aluminum stubs with the help of adhesive carbon tape and were observed by environmental scanning electron microscopy (Quanta FEG 250, Thermo Scientific, Toronto, ON, Canada). The thickness of the hydrated membranes was evaluated from the acquired images by ImageJ software. Seven randomly chosen regions of ELR-membranes prepared at each concentration were measured.

2.5.3 Scanning electron microscopy (SEM)

ELR-membranes were N_2 cryogenized, freeze-dried and imaged by a field emission gun-scanning electron microscope FEG-SEM (JEOL 6500 SEC unit, Thermo Scientific, Toronto, ON, Canada). The pore size was measured from the freeze-dried membranes by ImageJ software. Ten randomly chosen regions of ELR-membranes prepared at each concentration were measured.

2.6 Diffusion studies

Diffusion assays were performed by fixing the ELR-membranes prepared at 50, 25 and 10 mg mL^{-1} between the recipient and the donor compartment of a Franz cell glass device (dimensions in Figure S2) purchased from Afora® (Barcelona, Spain). In order, phosphate buffered saline (PBS) was added to the recipient compartment, the ELR-membrane was clamped between the two compartments and the donor compartment was filled with the required FITC-dextran solution.

Five different molecular weights were chosen for the study (4, 20, 40, 70 and 150 kDa) performing the assay at 37°C further covering the donor and recipient chamber for preventing evaporation. At 8 hours, 1, 3, 6, 9, 12, 15, 18 and 21 days, a 20 µl volume was pipetted from the lower compartment. The selected time points allowed reaching a plateau in the polysaccharide diffusion. The increase in fluorescence suffered in the receiving solution was measured using a SpectraMax M2e Microplate Reader (Molecular Devices, San Jose, CA, USA) in the excitation and emission wavelengths of 493 and 520 nm, respectively. Following, the correspondent increase of the FITC-dextran concentration was calculated, normalized against the value at equilibrium (C_{max}) and plotted against time. This study was further performed with the ELR-membrane prepared at 5 mg mL^{-1}, in contrast these soft membranes were torn during the mounting step, thus providing unreliable diffusion data. Three diffusion experiments were performed for each ELR-membrane and FITC-Dextran molecule.

2.7 Kinetic model – study of the effective diffusion coefficient D_{Eff}

Effective diffusion coefficients (D_{Eff}) of the 50, 25 and 10 mg mL^{-1} ELR-membranes in presence of a set of FITC-dextran molecules (4, 20, 40, 70 and 150 kDa) were obtained according to the equations obtained by Bent and co-workers for Franz cell chambers[24]:

$$D_{Eff} = -\frac{Ah(V_{donor}+Ah+V_{receptor})}{t(V_{donor}+Ah/2)(V_{receptor}+Ah/2)} ln\left(1-\frac{C_{receptor}}{N/V_{donor}+Ah+V_{receptor}}\right) \quad (1)$$

Where A is the effective area of diffusion, h the height of the membrane, V_{donor} and $V_{receptor}$ represent the respective volume of the Franz cells compartments, t is the time, $C_{receptor}$ the concentration on the receptor chamber and N the total mass of the diffused molecules. Theoretical diffusion coefficient D_0 of the FITC-dextrans in PBS were calculated employing the Stokes-Einstein expression:

$$D_0 = \frac{k_B T}{6\pi\eta r} \quad (2)$$

Where k_B is the constant of Boltzmann, T is the temperature in degrees Kelvin, η is the viscosity and r represents the radius of the compound. Following, the D_{Eff}/D_0 ratios for each ELR-membranes and FITC-dextran were further determined.

2.8 Mechanical properties

Young's modulus, tensile strength and strain at break of the ELR-membranes prepared at 50, 25, 10 and 5 mg mL^{-1} were evaluated by performing a uniaxial test at r.t. (0.5 mm/s rate) with an Electroforce 5500 series (TA instruments, Newcastle, DE, USA) equipped with a 250 g load cell.

2.9 Statistical analysis

Two-way analysis of variance (ANOVA) with post-hoc Tukey test was used for analyzing the data employing the GraphPad Prism 7 (GraphPad software, La Jolla, CA, USA). Statistical significance codes were described as follows: *ns* $p > 0.05$; *$p \leq 0.05$; **$p < 0.01$.

3. RESULTS AND DISCUSSION

3.1 ELR-membrane: Components

Two complementary ELRs, namely VKV-cyclooctyne and the de-novo designed SKS-azide, were employed for fabricating click-crosslinked ELR-membranes at the interface of a two-phase system. Twenty-four lysine amino acids were encoded along both polypeptide backbones while, in case of the SKS, eighty-four serine groups were further interspersed. These guest amino acids served different purposes, namely lysine primary amines acted as anchorage points for tethering the crosslinking reactive groups while serine β-hydroxyl groups increased the polarity and so the T_t of the SKS construct. This newly produced SKS ELR, intended to be loaded in the aqueous phase, was expressed in *E. coli* bacteria and purified according to well established protocols[22].

Tt and the variation of enthalpy associated to the SKS-azide phase transition. (d) FTIR and (e,f) ^{1}H NMR spectra with the signals corresponding to the tethered azide groups, namely 2107 cm^{-1} in the infrared spectrum and A, B, C and D in the ^{1}H NMR.

The purity of the polypeptide was checked by SDS-PAGE analysis (Figure S1A) while the correct amino acid composition and molecular weight were corroborated by HPLC (Figure S1B) and MALDI-TOF (Figure 1A), respectively. The intended increase in the T_t, attributed to the interspersed serine residues[25], was confirmed by DSC. The polar β-hydroxyl groups prevented the characteristic hydrophobic folding of the ELR chain in aqueous media below 70°C (Figure 1C).

The T_t, as well as the molecular weight, were altered once in the azide-modified version. The introduction of azide groups produced an increase in the found peaks by MALDI-TOF spectrometry (Figure 1B), while the partly disappearance of positively charged primary amines decreased the hydrophilicity of the ELR affording a T_t peak at 34.2°C in the thermogram (Figure 1C).

FTIR and ^{1}H NMR analysis further allowed identifying the tethered click-reactive groups. As such, a peak in the infrared region centered at 2100 cm^{-1} confirmed the presence of the azide groups (Figure 1D), while a series of ^{1}H NMR signals, associated to the lysine-azide linker, provided the substituted percentage of lysines within the SKS backbone (75%) (Figure 1E-F).

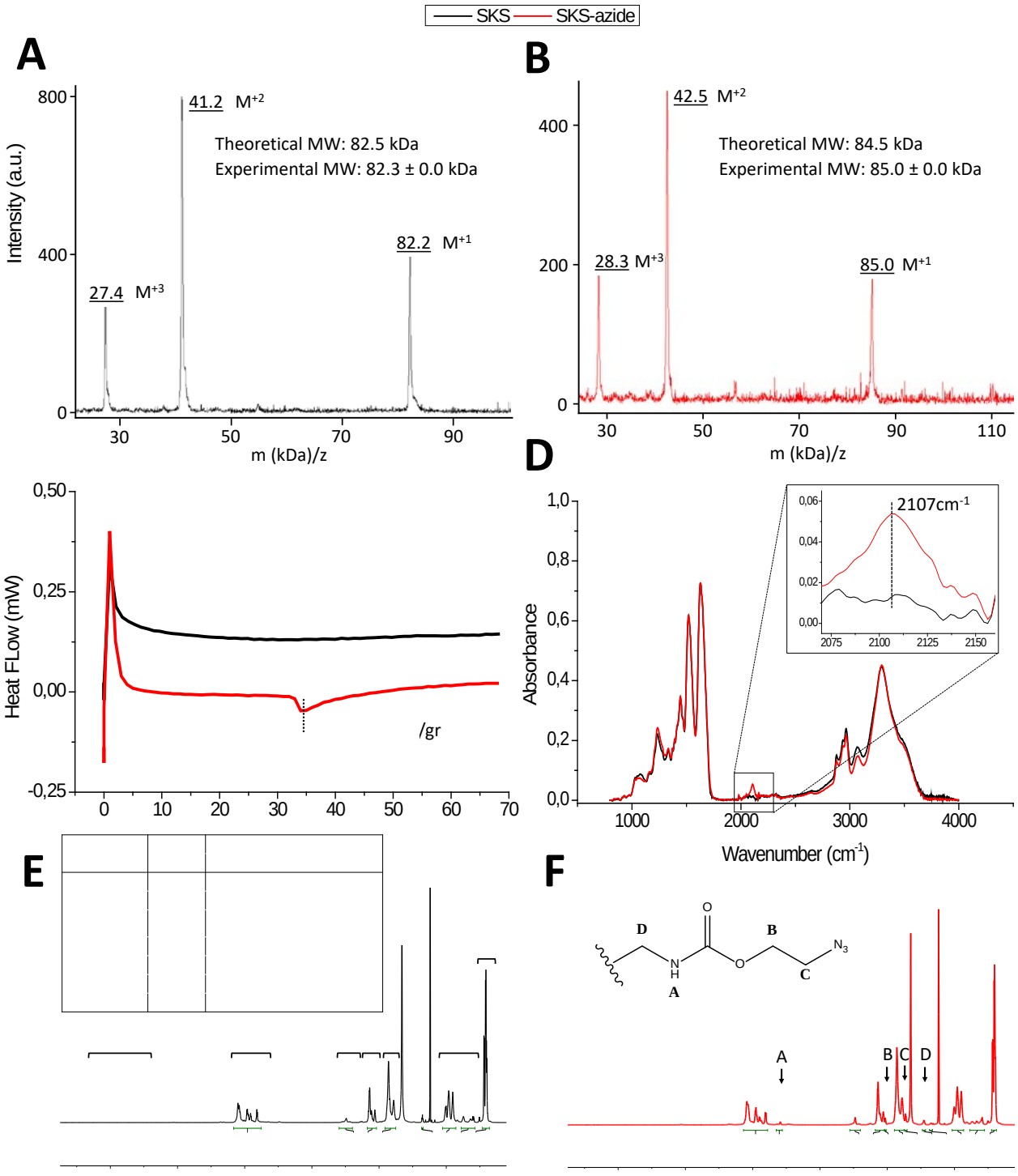

Figure 1. Chemical characterization of the SKS (black) and SKS-azide (red) ELRs. (a,b) MALDI-TOF spectrum with the mono- (M^{1+}), di- (M^{2+}) and tri-charged (M^{3+}) states. (c) DSC

thermogram accompanied by the Tt and the variation of enthalpy associated to the SKS-azide phase transition. (d) FTIR spectra accompanied by an insert highlighting the signal corresponding to the tethered azide groups to the SKS-azide at 2107 cm^{-1}. (e,f) ^{1}H NMR spectra were A, B, C and D represent the signals associated to the azide groups introduced in the SKS-azide and the broad peak at 3.3 ppm arises from traces of mono-deuterated and pure water (HOD and H2O) from the solvent. Experimental ("Exp") number of ^{1}H and theoretical values ("Th") are shown in a table.

Following, the adequate water-immiscible and VKV-cyclooctyne solubilizing organic phase was studied. As showed in the Table 1, 12 solvents were assayed against the complementary VKV-cyclooctyne.

Solvent	Relative polarity[26]	VKV-cyclooctyne solubility
Dioctyl ether	-	N
Xylene	0.074	N
Diethyl ether	0.117	N
Ethyl acetate	0.228	N
Chloroform	0.259	N
3-pentanone	0.265	N
Cyclohexanone	0.281	N
Dichloromethane	0.309	N
Dimethylsulfoxide (DMSO)$^{\mathbf{M}}$	0.444	Y
1-pentanol	0.568	N
Ethyl acetoacetate	0.577	N
n-butanol (BuOH)	0.586	N
Water$^{\mathbf{M}}$	1.000	Y

Table 1. List of the solvents selected for the miscibility studies in presence of the VKV-cyclooctyne. The relative polarity and ability of a set of solvents for dissolving the VKV-cyclooctyne ELR are represented in the second and third column of the table, respectively. M identifies those solvents miscible with water, whereas N and Y identify those solvents unable and able to dissolve the VKV-cyclooctyne, respectively.

Due to the singular character of the click-modified VKV-cyclooctyne ELR, no water-immiscible organic solvent able to dissolve the polypeptide was found. Thereby, a study comprising mixtures with the powerful ELR-solubilizing but water-miscible DMSO were explored. Interestingly, only BuOH/DMSO mixtures were able to dissolve the VKV-cyclooctyne ELR, finding an optimal proportion of 23% DMSO in BuOH that formed a biphasic system when mixed with water. This behavior was reasoned to be related with the BuOH ability for creating H-bonds, its high relative polarity[26] and long aliphatic chain.

In addition, the use of an organic phase for the corresponding VKV-cyclooctyne counterpart induced the suppression of the characteristic phase transition occurring in aqueous media. The found combination of solvents assured the preservation of the ELR versions in a solubilized and conformational free state at r.t. thus assuring the homogeneous crosslinking and formation of an ELR network at the liquid-liquid interface.

3.2 ELR-membrane: Formation and structure

Experimentally, putting in contact the complementary aqueous and organic ELR solutions triggered an intense chain of events at the liquid-liquid interface. As found by live imaging, ELR chains began to simultaneously crosslink in separated regions across the liquid surface producing the nucleation and sprouting of independent entities with time (see videos in supporting information). At this point, a phenomenon directed by the device walls was noticed. Once the crosslinked seeds kept in contact with the device wall, a driving force began pulling and expelling the crosslinked net from the wall (Figure S3A and S3B). A possible explanation for this particular effect could be related with the covalent click reaction, the convection currents produced at the liquid interface and the stickiness of polypeptides to common materials such as plastic and glass.

Such progressions produced violent collisions against others proto-membranes coming from identical events happening in referable points distributed along the interface. Crosslinked networks began to interconnect between each other since the very first second they meet guiding the formation of a continuous matrix over time. This intense and dynamic pathway promoted the evolution of dense fiber-like clusters across the eventual ELR-membrane surface (Figure 2A).

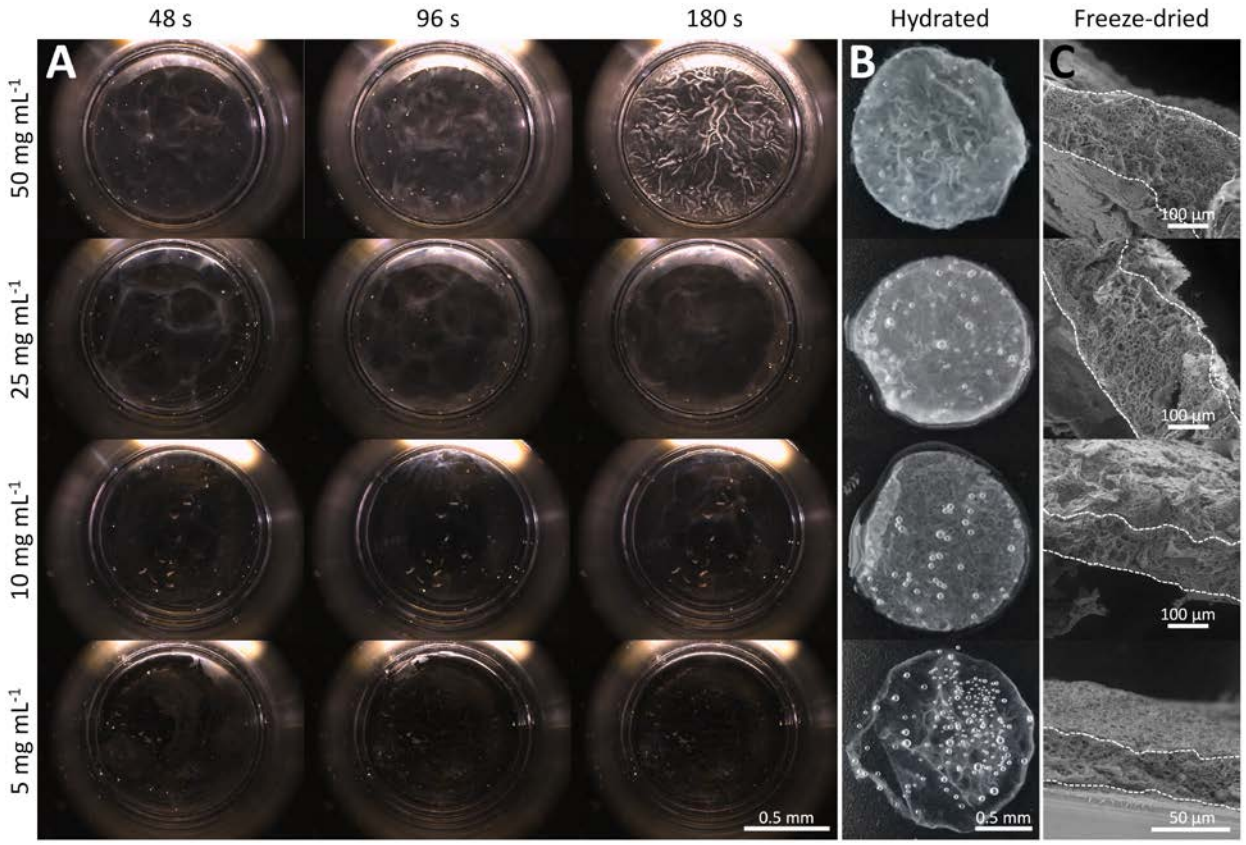

Figure 2. Morphological characterization of the fabricated ELR-membranes at 50, 25, 10 and 5 mg mL^{-1}. (a) Representative images of ELR-membrane formation with time. (b) Representative images of the isolated and hydrated ELR-membranes. (c) Representative SEM images of the freeze-dried and cryo-fractured ELR-membranes where the cross-section borders appear highlighted by a white dashed line.

Recorded videos further showed the upregulation of the ELRs reaction-diffusion rate by the initial concentration. Larger amounts of available ELR chains at both sides of the liquid interface strongly promoted the diffusion, crosslinking and ELR-membrane formation process. The progressive formation of a network gradually hampered the diffusion of ELR chains at the interface thus reducing to an almost negligible speed the reaction-diffusion process over time. This process was fostered with the increasing concentration of the ELR solutions finding denser membrane-like networks at shorter times (Figure 2A).

In accordance with the proposed formation pathway, the simultaneous formation and growth of independent aggregates across the interface create dense regions along the liquid-liquid interface. While the subsequent coalescence of these structures created thin interconnecting matrixes thereby conferring the observed rough appearance to the surface of the fabricated membranes (Figure S4).

An important feature of the obtained ELR-membranes was their inner translucency. This property showed to be regulated with the initial concentration obtaining more opaque membranes as this parameter was increased (Figure 2B). As examined by scanning electron microscopy techniques, higher concentrations gave rise to smaller pore size distributions and thicker thicknesses (Figure 3), thus originating this phenomenon.

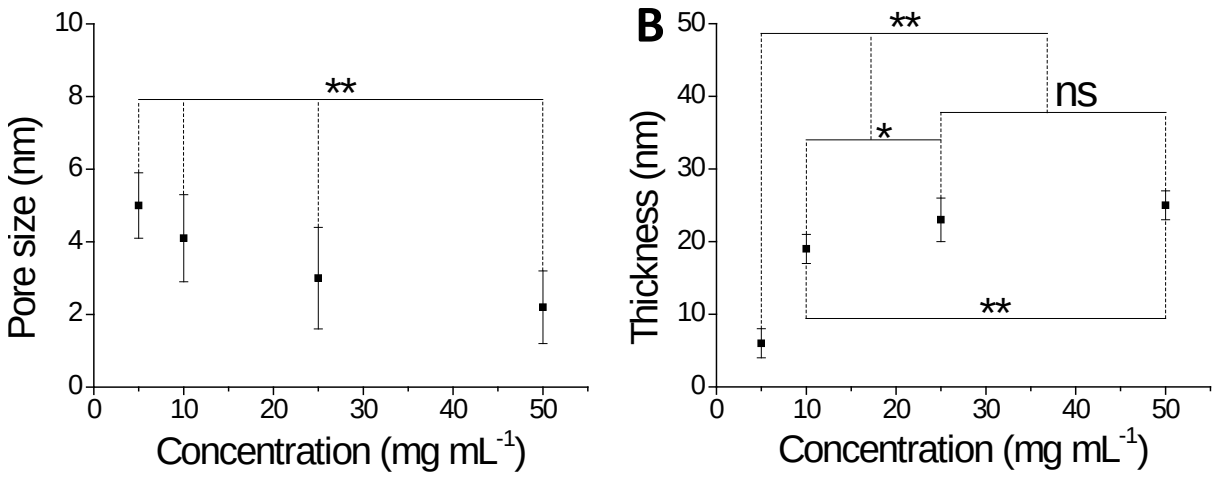

Figure 3. Membrane thickness and pore size. (a) Pore size and (b) thickness of the 50, 25, 10 and 5 mg mL^{-1} ELR-membranes measured on their hydrated and freeze-dried state, respectively. Error bars correspond to the standard deviation. ** stands for $p < 0.01$, * for $p \leq 0.05$ and *ns* for $p > 0.05$.

The internal microstructure was investigated observing the freeze-dried ELR-membranes by scanning electron microscopy (SEM) (Figure 2C). As found, an interconnected and porous morphology dominated the interior of the structures matching with the previously reported appearance for covalent-crosslinked ELR-hydrogels[17, 21, 27]. This irregular morphology supported the hypothesized mechanism for the interface membrane formation while the absence of channels connecting both faces of the ELR-membrane corroborated the advance of the crosslinking process until the complete coverage of the liquid-liquid interface.

Cross-section images further reported the relationship between the pore size and the thickness with the initial concentration (Figure 3). Even though ELR-membranes showed a large pore size distribution, their size tended to decrease with the increasing concentration (** $p < 0.01$). Presumably, this effect was correlated with the formation process. Higher concentrations should

increment the junction points employed by the ELR chains to interconnect thus forming a denser matrix. Moreover, along with this effect, an increase on the thickness of the membranes was observed (Figure 3B). We reason that increasing the amount of material accelerated the growing stage thereby hampering the horizontal arrangement of the forming independent networks while promoting the reaction-diffusion process in the perpendicular direction to the liquid-liquid interface. In addition, the thicknesses exhibited by the 25 and 50 mg mL^{-1} membranes were virtually identic (*ns* $p > 0.05$). This result supported the suggested formation process prompting out the barrier effect produced by the forming ELR membrane over the diffusion and crosslinking reaction of ELR chains at the interface.

3.3 ELR-membrane: Diffusion properties

The identified sponge-like conformation anticipated the feasible hampering properties over the diffusion of molecules in solution. In order to numerically evaluate the ELR-membrane potential as a diffusion-controlling system for biological environments, a study comprising Franz cells at physiological conditions (PBS at 37°C) was performed. Due to the vast set of compounds that can be found in a living organism, e.g. molecules from a few Daltons to proteins with higher molecular weight than the ELRs themselves, a set of five fluorescent-labelled dextran molecules from 4 to 20, 40, 70, and 150 kDa were selected. These polysaccharides serve as models for the behavior of molecules of interest such as the immunoglobulin G (MW 150 kDa), the glycoprotein transferrin (MW 81 kDa), the bovine serum albumin (MW 66 kDa), the ovalbumin (MW 45 kDa), the cytokine interleukin 1 beta (MW 17.5k Da) and the hormone insulin (MW 5.8 kDa). Furthermore, as the effective hydrated radius of these molecules in solution is already known, we were able to approximately predict future diffusion histories of similar-sized molecules displaying hydrodynamic radius (R_H) of 14, 33, 45, 60 and 85 Å, respectively.

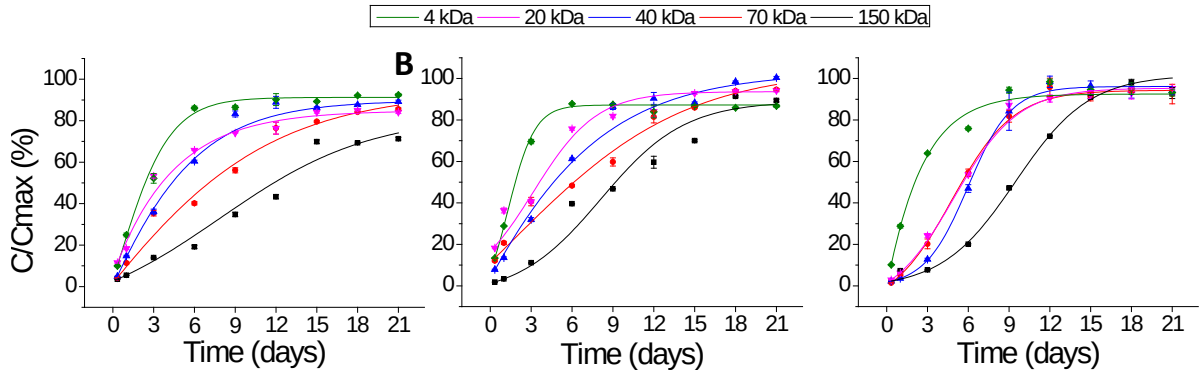

Figure 4. Franz cells diffusion experiments. Diffusion curves of the corresponding 4 (green), 20 (purple), 40 (blue), 70 (red) and 150 (black) kDa FITC-dextran molecules in presence of the (a) 50, (b) 25 and (c) 10 mg mL^{-1} ELR-membranes representing the normalized concentration (diffused concentration against the concentration at infinite time, C/C_{max}) versus time. Error bars correspond to the standard deviation.

Positively, diffusion experiments demonstrated the ability of ELR-membranes to selectively control the mass transfer rate of FITC-dextrans by means of molecular weight (Figure 4). Interestingly, although the 50, 25 and 10 mg mL^{-1} ELR-membranes displayed a referable logarithmic to sigmoidal profile with the increasing molecular weight (from 4 to 150 kDa), a different rate in the diffusion kinetics was noticed between them.

The greater amount of crosslinked ELR chains composing the thicker structure of the 50 mg mL^{-1} membrane forced the dextran molecules to follow a sinuous path through the membrane. This configuration produced a braking effect lowering the mass diffusion rate. While a half diffusion time of 2.8 days was obtained for the smallest molecule (4 kDa), 10.8 days were required for the largest molecule of 150 kDa (Figure 4A). The diffusion kinetics were accelerated once in presence of the 25 mg mL^{-1} ELR-membrane (Figure 4B). The thinner structure and larger pore size smoothed the diffusion of the molecules shortening the elapsed time for crossing the membrane

barrier. As found, half diffusion times decreased to 2.6 and 9.8 days for the 4 and 150 kDa, respectively. This effect was replicated for the 10 mg mL^{-1} ELR-membrane (Figure 4C). The thinner and less dense character favored the permeation of the particles in solution thus obtaining half diffusion times of 2.8 and 9.3 days for the 4 and 150 kDa, respectively. Negatively, Franz cell mounting step disrupted the integrity of the 5 mg mL^{-1} ELR-membranes impeding performing the diffusion study for this condition. This result was attributed to the highly soft and thin character of this membrane that was translated into a poor compliance and difficult handling for the built construct.

According to Fick's laws, the effective diffusion coefficients (D_{Eff}) were obtained for the ELR-membranes (Figure 5B). Complementarily, in order to evaluate the inhibitory effect over the free diffusion of the studied molecules in PBS, the ratio against the theoretical diffusion coefficients (D_{Eff}/D_0) was calculated. As found, effective diffusion rates (D_{Eff}) showed to reach a difference in the range of three orders of magnitude when compared to the theoretical diffusion coefficients (D_0) (Figure 5A). Moreover, the graph showed a similar logarithmic trend for the three ELR-membranes with the difference focused on the initial steepness of the curve and the steady value reached for the plateau.

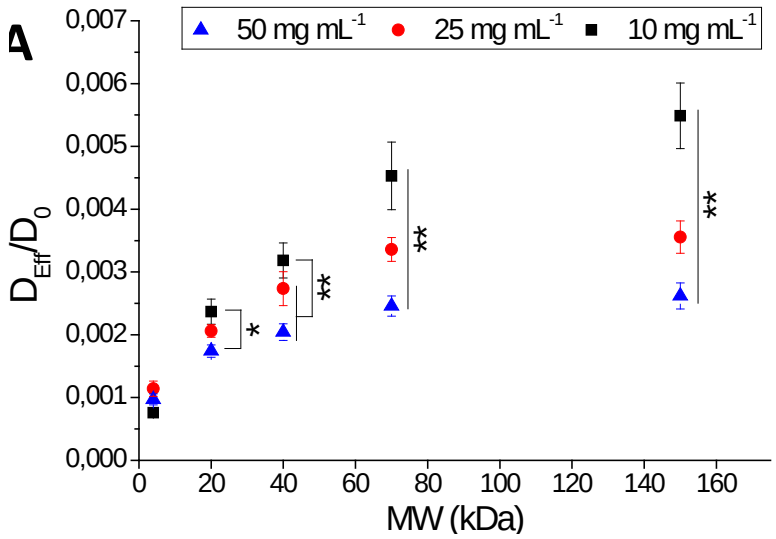

	FITC-Dextran		50 mg mL^{-1} ELR-membrane		25 mg mL^{-1} ELR-membrane		10 mg mL^{-1} ELR-membrane	
MW (kDa)	R_H (nm)	D_0 (x 10^{-11} m^2 s^{-1})	D_{Eff} (x 10^{-13} m^2 s^{-1})	D_{Eff}/D_0 (x 10^{-3})	D_{Eff} (x 10^{-13} m^2 s^{-1})	D_{Eff}/D_0 (x 10^{-3})	D_{Eff} (x 10^{-13} m^2 s^{-1})	D_{Eff}/D_0 (x 10^{-3})
150	8.5	3.9	1.0 ± 0.08	2.6 ± 0.2	1.4 ± 0.1	3.6 ± 0.3	2.1 ± 0.2	5.5 ± 0.5
70	6	5.5	1.4 ± 0.09	2.5 ± 0.2	1.8 ± 0.1	3.4 ± 0.2	2.5 ± 0.3	4.5 ± 0.5
40	4.5	7.3	1.5 ± 0.1	2.0 ± 0.1	2.0 ± 0.2	2.7 ± 0.3	2.3 ± 0.2	3.2 ± 0.3
20	3.3	10.0	1.8 ± 0.1	1.8 ± 0.1	2.1 ± 0.1	2.1 ± 0.1	2.4 ± 0.2	2.4 ± 0.2
4	1.4	23.5	2.3 ± 0.2	1.0 ± 0.09	2.7 ± 0.3	1.1 ± 0.1	1.8 ± 0.1	0.8 ± 0.04

Figure 5. Evaluation of the effective diffusion coefficient (D_{Eff}). (a) Ratio between the effective and theoretical diffusion coefficient (D_{Eff}/D_0) of the FITC-dextran molecules in presence of the 50 (blue), 25 (red) and 10 (black) mg mL^{-1} ELR-membranes as function of the polysaccharide molecular weight. (b) Molecular weight, hydrodynamic radius and theoretical diffusion coefficients of the FITC-dextran polysaccharides in PBS (D_0) are presented in the first three columns. Diffusion coefficients for the 50, 25 and 10 mg mL^{-1} ELR-membranes (D_{Eff}) and the respective D_{Eff}/D_0 ratios are shown in the remaining columns. Error bars correspond to the standard deviation. ** stands for $p < 0.01$ and * for $p \leq 0.05$. (*ns* $p > 0.05$ was found for the comparisons not represented in the graph).

The lowest D_{Eff}/D_0 values were obtained at the beginning of the representation indicating a stronger inhibiting effect over the diffusion for the light dextrans (Figure 5A). The decelerating effect over the diffusion kinetics was stronger maintained as the thickness of the ELR-membrane increased and the pore size decreased. This trend towards a plateau over time suggested that permeability of heavier polysaccharides than the assayed would provide D_{Eff}/D_0 ratios in the order of the values obtained for the 150 kDa dextran for each ELR-membrane. Additionally, the reported values may allow estimating the response of ELR-membranes prepared at different concentrations within the studied window.

The 50 mg mL^{-1} ELR-membrane showed the highest performance in presence of the largest molecules (150, 70 and 40 kDa) once compared to the 25 and 10 mg mL^{-1} ELR-membranes (**$p < 0.01$). This effect presumably resulted from the steric hindrance exerted by the dense arrangement displayed by the 50 mg mL^{-1} membrane. Interestingly, reducing to the half the concentration for preparing the membrane (25 mg mL^{-1}) provided no difference once controlling the diffusion of the 20 kDa dextran (*ns* $p > 0.05$). This result proved beneficial the use of the 25 mg mL^{-1} ELR-membrane for controlling the diffusion of intermediate molecules thus saving material in the fabrication of the constructs.

On the contrary, whereas the 10 mg mL^{-1} ELR-membrane depicted the fastest diffusion rate for the 70 and 150 kDa molecules (**$p < 0.01$, Figure 5A) this trend was inverted with the decreasing size and molecular weight. As found, no statistically difference was obtained between the three ELR-membranes and the 4 kDa FITC-dextran (*ns* $p > 0.05$). Indeed, the smallest D_{Eff}/D_0 ratio was achieved by this 10 mg mL^{-1} ELR-membrane. The low concentration at which this structure was prepared identified it as the cost-effective condition for decelerating and controlling the diffusion of small and light molecules (≈ 4 kDa). This result further demonstrated that the diffusion,

presumably guided by the osmotic pressure, not only was disturbed by the thickness and dense interconnected porous interior of the membrane but for specific molecule-membrane interactions as well.

The uncharged nature of the dextran molecules made feasible to hypothesize a diffusion kinetics governed by the interplay of hydrophobic and hydrophilic forces displayed by the multiple groups spread along the proteinaceous ELR backbone. Due to the employment of recombinant elastin-like building blocks, tailored ELR-membranes for the intended application could be envisaged. Thereby, by selecting the required polar, non-polar, positively or negatively charged amino acids, attractive or repulsive interactions in contact with the target molecule could be addressed in an elegant fashion.

Not only the adaptable nature of the described ELR-membranes resulted of interest. Their exhibited D_{Eff} values, namely in the range of 2 $x10^{-13}$ m^2 s^{-1}, further evidenced a valuable performance once compared to referable biomaterial-built systems described in the literature. Popa and colleagues[28] developed a 0.8 mm height transparent atelocollagen-oxidized hydrogel for encapsulating stromal cells with diffusion coefficients, once in presence of albumin (66.2 kDa), between 1 and 0.5 $x10^{-12}$ m^2 s^{-1}. Photocrosslinked poly(ethylene glycol) 0.7 mm thick hydrogels designed by the group of Frank et al. showed comparable D_{Eff} values of 10 and 1 $x10^{-12}$ m^2 s^{-1} in presence of two proteins weighting 17 and 150 kDa, respectively[29]. Referable crosslinked 0.5 mm thick dextrin hydrogels showed a D_{Eff} of 4 $x10^{-11}$ m^2 s^{-1} for BSA (67 kDa) and 11 $x10^{-11}$ m^2 s^{-1} when employing glucose (180 Da)[30]. Chitosan and alginate-based membranes, showing a thickness of 0.2 mm, reported D_{Eff} values around 2 $x10^{-10}$ m^2 s^{-1} in presence of sugars lighter than 1 kDa[31, 32], while polycarbonate membranes exhibited values from 7 to 3 $x10^{-11}$ m^2 s^{-1} with PEG and dextran molecules weighting from 10 to 62 kDa[33].

Alternatively, other approaches exploited the fabrication of salt-sensitive or biologically-degradable capsules able to modulate the delivery rate depending on the added amount of rupturing-agent[34-36]. Interestingly, a similar feature can be implemented in our system as well. As described[37, 38], the recombinant origin and versatile nature of the ELR also allows introducing biodegradable sequences in their proteinaceous backbone thereby opening the possibility for fabricating membranes with moldable diffusion properties in response to specific external factors.

3.4 ELR-membrane: Mechanical characterization

The elastic modulus (Young's modulus), strength and strain at break displayed by the ELR-membranes were evaluated by a uniaxial test to failure (Figure S5).

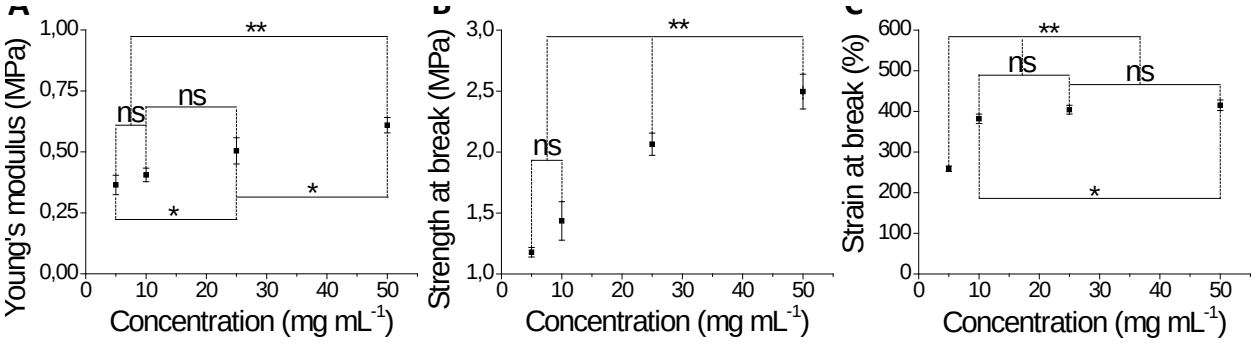

Figure 6. Mechanical characterization. (a) Young's modulus, (b) tensile strength at break and (c) strain at break are represented versus the ELR-membrane concentration, namely 5, 10, 25 and 50 mg mL^{-1}. Error bars correspond to the standard deviation. ** stands for $p < 0.01$, * for $p \leq 0.05$ and *ns* for $p > 0.05$.

As a general trend, the decrease in ELR-membrane concentration produced a progressive fall on the mechanical properties (Figure 6). Accordingly, the 50 mg mL^{-1} ELR-membrane doubled the elastic modulus exhibited by the 5 mg mL^{-1} membrane (** $p < 0.01$) while 10 and 25 mg mL^{-1}

conditions covered the gap depicting a gradual decay (Figure 6A). Contrarily, a more accused tendency was noticed for the tensile strength at break (Figure 6B). The 50 and 25 mg mL^{-1} ELR-membranes withstood a stress in the order of 2 MPa before failure, evidencing a pronounced decrease for the 10 and 5 mg mL^{-1} membranes (** $p < 0.01$). This decay was specially accused for the 5 mg mL^{-1} membrane strain at break (Figure 6C). Whereas the 50, 25 and 10 mg mL^{-1} membranes exhibited a value around 400% (*ns* $p > 0.05$) a strong drop in the strain at break was observed for the 5 mg mL^{-1} ELR-membranes (** $p < 0.01$). This result corroborated the difficulties encountered for measuring the diffusion properties of the 5 mg mL^{-1} membranes with the Franz cell. While, on the contrary, 50, 25 and 10 mg mL^{-1} ELR-membranes were found easy to handle constructs. Interestingly, being able to manipulate the fabricated ELR-membranes widens their applicability thus preventing their rupture and assuring their integrity in harsh environments with time.

The effect of the liquid-liquid interface and the click crosslinking approach over the mechanical properties of the built membranes can be deeply understood by comparison with previously described technologies for the fabrication of ELR matrixes. In this sense, electrospun and catalyst-free click crosslinked ELR fibers, prepared at 50 mg mL^{-1}, exhibited stiffer mechanical properties, i.e. higher elastic modulus (≈ 1,73 MPa) accompanied by a lower tensile strength (≈ 0.59 MPa) and strain at break (≈ 248%)[39].

Alternative, casting techniques comprising the use of less cytocompatible crosslinking approaches, based on hexamethylene diisocyanate (HDMI)[40] and glutaraldehyde (GTA)[41], or by the cytocompatible and photocrosslinkable cysteines[42], have further served for the fabrication of ELR films at concentrations of 100 mg mL^{-1}. As such, HDMI crosslinked networks offered higher values of strength at break (4MPa) while resembled the young modulus and strain at break values

offered by the 50 mg mL^{-1} ELR-membranes, i.e. in the range of 0.6 MPa and 400% respectively. On the other hand, GTA crosslinked films displayed a lower elastic modulus and tensile strength (ca. 0.2 and 0.9 MPa, respectively) but mirrored the elongation at break (≈ 400%). In the last photocrosslinkable scenario, the limited number of anchoring of points, i.e. a pair of cysteine groups per ELR chain, rendered elastic modulus and ultimate strength values one order of magnitude lower, i.e. in the range of kPa. Nevertheless, a similar strain at break was displayed (around 400%).

These comparisons identified the developed approach as a powerful tool for providing with elastic and resilient properties to the thin ELR-membranes. Indeed, the reported elastic moduli were in the order of those displayed by the native elastin, namely 0.3 to 0.6 MPa, whereas the values of strain at break, except for the 5 mg mL^{-1} condition, double the native value (100-220%)[5]. This mismatch was presumably attributed to the entangled microfibrils constituting the elastic fibers which could act limiting the extensibility of the elastin[43].

Furthermore, as it was checked by differential scanning calorimetry, no sign of hydrophobic transition was found between 0 and 65°C for the ELR-membranes in PBS (Figure S6). This result assured the maintenance of the mechanical, translucency and diffusion properties under physiological conditions (37°C). Measured physical features, along with the demonstrated ability to introduce bioactive RGD cell-adhesive motifs within the membrane backbone, proved the potential applicability of the designed technology for developing biochemical and mechanical tailorable diffusion devices from ELR peptides. In this regard, the reported relation between the exhibited properties and the employed concentration further allows to hypothesize the fabrication of thicker ELR-membranes with higher mechanical and diffusion properties.

4. CONCLUSIONS

We have developed an innovative technology for manufacturing tunable and potentially cyto and biocompatible click-crosslinkable ELR-membranes at a liquid-liquid interface. Live characterization showed the spontaneous appearance of proto-membrane entities that grow and interconnect building wrinkled constructs. The sponge-like structure, dominating the interior of the ELR-membranes, conferred with notable diffusion properties to the fabricated systems lowering the theoretical diffusion coefficient (D_0) of molecules up to 150 kDa in three orders of magnitude. Furthermore, the covalent crosslinking approach provided the proper mechanical strength to the thin fabricated ELR-membranes. Altogether, the collected results evidenced the designing of an original approach for producing moldable ELR-membranes in terms of shape, thickness, porosity, diffusive and mechanical properties. The high versatility of the employed elastin-like recombinamers opens up the possibility for further developing advanced membrane-like diffusion scaffolds with tunable biological and mechanical properties.

5. SUPPORTING INFORMATION

Physicochemical characterization of the SKS and SKS-azide ELRs by SDS-PAGE, HPLC, MALDI-TOF, DSC, ATR-FTIR and ^{1}H NMR techniques accompanied by the ESEM images, DSC thermograms, recorded videos and captures of the growing ELR-membranes are available in the supporting information.

6. ACKNOWLEDGEMENTS

The authors are grateful for the funding from the Spanish Government (MAT2016-78903-R, RTI2018-096320-B-C22), the Ministerio de Educación, Cultura y Deporte para la Formación de Profesorado Universitario to MG (FPU15-00448), the Junta de Castilla y León (VA317P18), the

Interreg V A España Portugal POCTEP (0624_2IQBIONEURO_6_E), the Centro en Red de Medicina Regenerativa y Terapia Celular de Castilla y León.

7. ABBREVIATIONS

ELRs, elastin-like recombinamers; DMSO, dimethyl sulfoxide; EtOH, ethanol; BuOH, n-butanol; Tt, transition temperature; SDS-PAGE, sodium dodecyl sulphate polyacrylamide gel electrophoresis; MALDI-TOF, matrix assisted laser desorption/ionization time-of-flight; FTIR, Fourier transform infrared spectroscopy; DSC, differential scanning calorimetry; ^{1}H NMR, proton nuclear magnetic resonance spectroscopy; PBS, phosphate buffered saline; SEM, Scanning electron microscopy; ESEM, environmental scanning electron microscopy; D_{Eff}, effective diffusion coefficient; D_0, theoretical diffusion coefficient; R_H, hydrodynamic radius; kDa, kiloDalton; HDMI, hexamethylene diisocyanate; GTA, glutaraldehyde.

8. REFERENCES

1. Qadir, D.; Mukhtar, H.; Keong, L. K., Mixed Matrix Membranes for Water Purification Applications. *Separation & Purification Reviews* **2017,** 46, (1), 62-80.
2. Buonomenna, M. G.; Bae, J., Organic Solvent Nanofiltration in Pharmaceutical Industry. *Separation & Purification Reviews* **2015,** 44, (2), 157-182.
3. Leijnse, N.; Jeon, J. H.; Loft, S.; Metzler, R.; Oddershede, L. B., Diffusion inside living human cells. *The European Physical Journal Special Topics* **2012,** 204, (1), 75-84.
4. Jornitz, M. W., *Filtration and purification in the biopharmaceutical industry*. CRC Press: 2019.
5. Fung, Y.-c., *Biomechanics: mechanical properties of living tissues*. Springer Science & Business Media: 2013.
6. Lieleg, O.; Ribbeck, K., Biological hydrogels as selective diffusion barriers. *Trends in Cell Biology* **2011,** 21, (9), 543-551.
7. Wise, S. G.; Weiss, A. S., Tropoelastin. *The International Journal of Biochemistry & Cell Biology* **2009,** 41, (3), 494-497.
8. Rauscher, S.; Pomès, R., The liquid structure of elastin. *eLife* **2017,** 6, e26526.
9. Urry, D. W., Molecular Machines: How Motion and Other Functions of Living Organisms Can Result from Reversible Chemical Changes. *Angewandte Chemie International Edition in English* **1993,** 32, (6), 819-841.

10. Muiznieks, L. D.; Sharpe, S.; Pomès, R.; Keeley, F. W., Role of Liquid–Liquid Phase Separation in Assembly of Elastin and Other Extracellular Matrix Proteins. *J. Mol. Biol.* **2018,** 430, (23), 4741-4753.
11. Vindin, H.; Mithieux, S. M.; Weiss, A. S., Elastin architecture. *Matrix Biology* **2019,** 84, 4-16.
12. Ibáñez-Fonseca, A.; Flora, T.; Acosta, S.; Rodríguez-Cabello, J. C., Trends in the design and use of elastin-like recombinamers as biomaterials. *Matrix Biol.* **2019,** 84, 111-126.
13. Mendes, A. C.; Smith, K. H.; Tejeda-Montes, E.; Engel, E.; Reis, R. L.; Azevedo, H. S.; Mata, A., Co-Assembled and Microfabricated Bioactive Membranes. *Adv. Funct. Mater.* **2013,** 23, (4), 430-438.
14. Mendoza-Meinhardt, A.; Botto, L.; Mata, A., A fluidic device for the controlled formation and real-time monitoring of soft membranes self-assembled at liquid interfaces. *Scientific Reports* **2018,** 8, (1), 2900.
15. Inostroza-Brito, K. E.; Collin, E.; Siton-Mendelson, O.; Smith, K. H.; Monge-Marcet, A.; Ferreira, D. S.; Rodríguez, R. P.; Alonso, M.; Rodríguez-Cabello, J. C.; Reis, R. L.; Sagués, F.; Botto, L.; Bitton, R.; Azevedo, H. S.; Mata, A., Co-assembly, spatiotemporal control and morphogenesis of a hybrid protein–peptide system. *Nature Chemistry* **2015,** 7, (11), 897-904.
16. Wu, Y.; Okesola, B. O.; Xu, J.; Korotkin, I.; Berardo, A.; Corridori, I.; di Brocchetti, F. L. P.; Kanczler, J.; Feng, J.; Li, W.; Shi, Y.; Farafonov, V.; Wang, Y.; Thompson, R. F.; Titirici, M.-M.; Nerukh, D.; Karabasov, S.; Oreffo, R. O. C.; Carlos Rodriguez-Cabello, J.; Vozzi, G.; Azevedo, H. S.; Pugno, N. M.; Wang, W.; Mata, A., Disordered protein-graphene oxide co-assembly and supramolecular biofabrication of functional fluidic devices. *Nature Communications* **2020,** 11, (1), 1182.
17. Testera, A. M.; Girotti, A.; de Torre, I. G.; Quintanilla, L.; Santos, M.; Alonso, M.; Rodríguez-Cabello, J. C., Biocompatible elastin-like click gels: design, synthesis and characterization. *Journal of Materials Science: Materials in Medicine* **2015,** 26, (2), 105.
18. Madl, C. M.; Katz, L. M.; Heilshorn, S. C., Bio-Orthogonally Crosslinked, Engineered Protein Hydrogels with Tunable Mechanics and Biochemistry for Cell Encapsulation. *Adv. Funct. Mater.* **2016,** 26, (21), 3612-3620.
19. Madl, C. M.; Heilshorn, S. C., Bioorthogonal Strategies for Engineering Extracellular Matrices. *Adv. Funct. Mater.* **2018,** 28, (11), 1706046.
20. Xu, Z.; Bratlie, K. M., Click Chemistry and Material Selection for in Situ Fabrication of Hydrogels in Tissue Engineering Applications. *ACS Biomaterials Science & Engineering* **2018,** 4, (7), 2276-2291.
21. González de Torre, I.; Santos, M.; Quintanilla, L.; Testera, A.; Alonso, M.; Rodríguez Cabello, J. C., Elastin-like recombinamer catalyst-free click gels: Characterization of poroelastic and intrinsic viscoelastic properties. *Acta Biomaterialia* **2014,** 10, (6), 2495-2505.
22. Rodríguez-Cabello, J. C.; Girotti, A.; Ribeiro, A.; Arias, F. J., Synthesis of Genetically Engineered Protein Polymers (Recombinamers) as an Example of Advanced Self-Assembled Smart Materials. In *Nanotechnology in Regenerative Medicine: Methods and Protocols*, Navarro, M.; Planell, J. A., Eds. Humana Press: Totowa, NJ, 2012; pp 17-38.
23. Girotti, A.; Reguera, J.; Rodríguez-Cabello, J. C.; Arias, F. J.; Alonso, M.; Testera, A. M., Design and bioproduction of a recombinant multi(bio)functional elastin-like protein polymer containing cell adhesion sequences for tissue engineering purposes. *Journal of Materials Science: Materials in Medicine* **2004,** 15, (4), 479-484.

24. Lee, C. J.; Vroom, J. A.; Fishman, H. A.; Bent, S. F., Determination of human lens capsule permeability and its feasibility as a replacement for Bruch's membrane. *Biomaterials* **2006,** 27, (8), 1670-1678.
25. Urry, D. W.; Gowda, D. C.; Parker, T. M.; Luan, C.-H.; Reid, M. C.; Harris, C. M.; Pattanaik, A.; Harris, R. D., Hydrophobicity scale for proteins based on inverse temperature transitions. *Biopolymers* **1992,** 32, (9), 1243-1250.
26. Reichardt, C., *Solvents and Solvent Effects in Organic Chemistry*. 3rd, Updated and Enlarged Edition ed.; Wiley-VCH: 2003; p 653.
27. Fernández-Colino, A.; Wolf, F.; Keijdener, H.; Rütten, S.; Schmitz-Rode, T.; Jockenhoevel, S.; Rodríguez-Cabello, J. C.; Mela, P., Macroporous click-elastin-like hydrogels for tissue engineering applications. *Materials Science and Engineering: C* **2018,** 88, 140-147.
28. Luca, A.; Butnaru, M.; Maier, S. S.; Knieling, L.; Bredetean, O.; Verestiuc, L.; Dimitriu, D. C.; Popa, M., Atelocollagen-based Hydrogels Crosslinked with Oxidised Polysaccharides as Cell Encapsulation Matrix for Engineered Bioactive Stromal Tissue. *Tissue Engineering and Regenerative Medicine* **2017,** 14, (5), 539-556.
29. Kristin, E.; Curtis, W. F., Protein diffusion in photopolymerized poly(ethylene glycol) hydrogel networks. *Biomedical Materials* **2011,** 6, (5), 055006.
30. Carvalho, J. M.; Coimbra, M. A.; Gama, F. M., New dextrin-vinylacrylate hydrogel: Studies on protein diffusion and release. *Carbohydr. Polym.* **2009,** 75, (2), 322-327.
31. Waluga, T.; Scholl, S., Diffusion of Saccharides and Sugar Alcohol Sorbitol in Chitosan Membranes and Beads. *Chemical Engineering & Technology* **2013,** 36, (4), 681-686.
32. Dembczynski, R.; Jankowski, T., Characterisation of small molecules diffusion in hydrogel-membrane liquid-core capsules. *Biochem. Eng. J.* **2000,** 6, (1), 41-44.
33. Shao, J.; Baltus, R. E., Hindered diffusion of dextran and polyethylene glycol in porous membranes. *AlChE J.* **2000,** 46, (6), 1149-1156.
34. Iskakov, R. M.; Kikuchi, A.; Okano, T., Time-programmed pulsatile release of dextran from calcium-alginate gel beads coated with carboxy-n-propylacrylamide copolymers. *Journal of Controlled Release* **2002,** 80, (1), 57-68.
35. Wang, Z.; Qian, L.; Wang, X.; Yang, F.; Yang, X., Construction of hollow DNA/PLL microcapsule as a dual carrier for controlled delivery of DNA and drug. *Colloids and Surfaces A: Physicochemical and Engineering Aspects* **2008,** 326, (1), 29-36.
36. De Geest, B. G.; Déjugnat, C.; Verhoeven, E.; Sukhorukov, G. B.; Jonas, A. M.; Plain, J.; Demeester, J.; De Smedt, S. C., Layer-by-layer coating of degradable microgels for pulsed drug delivery. *Journal of Controlled Release* **2006,** 116, (2), 159-169.
37. Flora, T.; González de Torre, I.; Alonso, M.; Rodríguez-Cabello, J. C., Use of proteolytic sequences with different cleavage kinetics as a way to generate hydrogels with preprogrammed cell-infiltration patterns imparted over their given 3D spatial structure. *Biofabrication* **2019,** 11, (3), 035008.
38. Madl, C. M.; Katz, L. M.; Heilshorn, S. C., Tuning Bulk Hydrogel Degradation by Simultaneous Control of Proteolytic Cleavage Kinetics and Hydrogel Network Architecture. *ACS Macro Letters* **2018,** 7, (11), 1302-1307.
39. González de Torre, I.; Ibáñez-Fonseca, A.; Quintanilla, L.; Alonso, M.; Rodríguez-Cabello, J.-C., Random and oriented electrospun fibers based on a multicomponent, in situ clickable elastin-like recombinamer system for dermal tissue engineering. *Acta Biomaterialia* **2018,** 72, 137-149.

40. Nowatzki, P. J.; Tirrell, D. A., Physical properties of artificial extracellular matrix protein films prepared by isocyanate crosslinking. *Biomaterials* **2004,** 25, (7), 1261-1267.
41. Welsh, E. R.; Tirrell, D. A., Engineering the Extracellular Matrix: A Novel Approach to Polymeric Biomaterials. I. Control of the Physical Properties of Artificial Protein Matrices Designed to Support Adhesion of Vascular Endothelial Cells. *Biomacromolecules* **2000,** 1, (1), 23-30.
42. Zhang, Y.-N.; Avery, R. K.; Vallmajo-Martin, Q.; Assmann, A.; Vegh, A.; Memic, A.; Olsen, B. D.; Annabi, N.; Khademhosseini, A., A Highly Elastic and Rapidly Crosslinkable Elastin-Like Polypeptide-Based Hydrogel for Biomedical Applications. *Adv. Funct. Mater.* **2015,** 25, (30), 4814-4826.
43. Mithieux, S. M.; Weiss, A. S., Elastin. In *Advances in protein chemistry*, Elsevier: 2005; Vol. 70, pp 437-461.